Structural Durability & Health Monitoring

Tech Science Press

https://doi.org/10.32604/sdhm.2026.087157

ARTICLE

Reflective Fiber Optic Angle Sensor for Monitoring the Rotation State of Monopolar Photovoltaic Tracking Mounts

Qingmin Hou[1], Guanghua Xiao[1] and Tongtong Dai[2,*]

[1]School of Smart City, Chengdu Vocational & Technical College of Industry, Chengdu, China
[2]Department of Mechanical Engineering, North China Electric Power University, Baoding, China

*Corresponding Author: Tongtong Dai. Email: 52452574@ncepu.edu.cn

Received: 11 June 2026; Accepted: 29 July 2026; Published: 24 August 2026

ABSTRACT: To address the issue of angular deviation in inclined single-axis photovoltaic tracking mounts during long-term operation-caused by wind disturbances, mechanical transmission gaps, installation inaccuracies, and environmental factors-a angle sensor based on reflective fiber-optic ranging principles has been developed for monitoring the rotation angle of the main shaft. This sensor employs a structural conversion approach of "using straight lines to replace curves", transforming the shaft's rotational angle into linear displacement of a mirror via a gear-rack mechanism, and generating corresponding output voltage signals through variations in reflected light intensity to measure rotation angles. Due to factors such as the optical response characteristics of reflective fiber probes, mechanical transmission gaps, assembly errors, and external environmental disturbances, a significant nonlinear relationship exists between the sensor's output voltage and rotation angle, making traditional linear fitting methods inadequate for accurately describing this complex input-output mapping relationship. To enhance angle inversion accuracy, this paper proposes a nonlinear modeling and error compensation method utilizing a two-stage neural network. First, a neural network model is established with sensor output voltage as input and standard angle values as output to capture the nonlinear relationship between voltage and angle. Subsequently, an error compensation model is constructed using output voltage and preliminary predicted angles as inputs, with prediction residuals as outputs, to perform secondary refinement of angle inversion results. Experimental results demonstrate that the average nonlinear error of the sensor was 31.96% without compensation; after applying the basic neural network angle inversion model, the nonlinear error decreased to 1.00%; further with two-stage neural network error compensation, it further decreased to 0.31%, representing a reduction of 0.69 percentage points compared to the basic model. On the 15 representative calibration points, the proposed method achieved an MAE of 0.401°, an RMSE of 0.425°, and a maximum error of 0.640°. For the independent measurement dataset used for final evaluation, the corresponding MAE, RMSE, and maximum error were 0.81°, 0.89°, and 1.40°, respectively.

KEYWORDS: Fiber optic angle sensor; two-stage neural network; nonlinear modeling; error compensation

1 Introduction

Photovoltaic (PV) tracking mounts are critical structural components in solar power plants for adjusting module orientation and enhancing power generation efficiency. Accurate determination of the main shaft rotation angle is essential for improving tracking control precision and ensuring safe operation of these mounts. A comprehensive review by Sadeghi et al. systematically classified solar trackers and emphasized that single-axis trackers achieve 20%–35% higher energy yield than fixed-tilt systems, while sensor technologies-including fiber-optic sensors-play a central role in determining tracking precision and

Copyright © 2026 The Authors. Published by Tech Science Press. This work is licensed under a Creative Commons Attribution 4.0 International License, which permits unrestricted use, distribution, and reproduction in any medium, provided the original work is properly cited.

environmental adaptability [1]. Sun et al. further demonstrated that deep neural network calibration can improve the accuracy of four-quadrant analog sun sensors from 1° to 0.1° (1σ), confirming the value of data-driven methods for angular sensing in solar tracking applications [2]. Angle sensors serve as key components for monitoring mount rotation; however, traditional potentiometric, magnetoresistive, inductive, and photoelectric encoding sensors still exhibit limitations under prolonged outdoor operation, complex electromagnetic environments, and distributed installation conditions [3]. Therefore, developing angle measurement methods with strong anti-interference capabilities, excellent structural adaptability, and ease of field installation is of significant importance.

Fiber optic sensors offer advantages such as excellent insulation properties, strong resistance to electromagnetic interference, compact size, lightweight construction, and long-distance signal transmission capabilities, making them ideal for structural condition monitoring in complex outdoor environments. In recent years, fiber optic sensing technology has been increasingly applied to detect physical parameters including angles, displacements, strains, currents, and temperatures. Early foundational work by Zhang et al. proposed a reflective fiber-based angle measurement system that converts rotational angles into linear displacement of mirrors, utilizing variations in reflected light intensity for angle detection [4]. Lee et al. demonstrated the application potential of plastic optical fibers for low-cost angle measurement in assessing the orientation of moving components [5]. To improve sensitivity and mitigate nonlinear decay, Jia et al. developed a differential reflective intensity optical fiber angular displacement sensor with a linear angular range of 74.4° and sensitivity of 0.051 V/° [6]. Extending the measurement range, Luo et al. proposed a fiber angular displacement sensor utilizing orbital angular momentum beam interference, achieving a sensitivity of 3524.158°/° within 0°–2° and 53.849°/° within 152°–2° [7]. For high-precision tilt monitoring, Pan et al. designed a high-sensitivity fiber Bragg grating (FBG) tilt sensor with sensitivity up to 231.7 pm/° and integrated silicone-oil vibration damping [8]; Zhang et al. further developed a dual-axis FBG tilt sensor based on a universal joint structure, achieving resolutions of approximately 4.4×10^{-4}° [9]; and Theophilus et al. recently proposed a sensitivity-enhanced FBG tilt sensor with 129.95 pm/° sensitivity and 0.9997 linearity over a −30° to 30° range [10]. These advances confirm that fiber-optic approaches-spanning intensity-modulated, FBG, and interferometric configurations-provide a robust technological foundation for angle monitoring in outdoor PV environments.

However, output signals from reflective fiber sensors are influenced by multiple factors-including the relative distance between the probe and reflective surface, reflection surface orientation, light source intensity, photoelectric conversion characteristics at the receiver, and mechanical transmission mechanisms. During angular monitoring of inclined single-axis solar tracking systems, measurement errors may arise from main shaft rotation, gear-rack clearance, installation deviations, outdoor lighting fluctuations, or environmental disturbances. Additionally, the relationship between reflected light intensity and distance does not follow strict linearity, resulting in significant nonlinearities between sensor output voltage and actual rotation angles. While traditional linear fitting or low-order polynomial methods simplify model construction, they fail to accurately capture the complex nonlinear characteristics across the entire measurement range, particularly under conditions of severe light intensity variations or pronounced mechanical hysteresis.

To enhance the modeling capability of sensor nonlinear outputs, machine learning and neural network approaches have been widely employed in recent years for sensor calibration and error compensation. Liu et al. utilized adaptive linear neurons to compensate for nonlinear and hysteresis errors in resistive angle sensors, significantly improving measurement accuracy [3]. Li et al. employed artificial neural networks to infer angular information from nonlinear optical signals, enabling nonlinear optical angle measurement [11]. Lin et al. further conducted measurement uncertainty analysis on optical angle sensors using multi-layer perceptron neural networks, demonstrating that while neural network models can improve angle inversion precision, their reliability must be validated through rigorous error evaluation methods [12]. Beyond angle measurement, neural networks demonstrate strong applicability in various nonlinear compensation tasks for sensors. Wei and Liu employed an improved optimization algorithm combined with a backpropagation (BP) neural network to compensate for temperature drift in MEMS accelerometers, significantly reducing nonlinear temperature-related errors [13]. Chen et al. applied neural network-assisted error compensation techniques to microfiber knot current sensors, demonstrating their feasibility for real-time error correction in such devices [14]. Cao et al. highlighted in a 2025 review that artificial intelligence methods have been widely utilized for complex output interpretation, noise reduction, demodulation optimization, and fault prediction in fiber optic sensors [15]. Zhou et al. demonstrated that machine learning applications in optical fiber sensing have become a research agenda, with ML algorithms increasingly used to tackle signal complexity and enable automated decision-making [16]. Tritschler et al. demonstrated that meta-learning approaches enhance sensor calibration adaptability under varying environmental conditions and individual variations through low-sample self-calibration [17]. Fan et al. employed a tangential functional link artificial neural network integrated with snake optimization to compensate for nonlinear errors in linear variable differential transducers, confirming that cascaded neural network structures can substantially outperform single-network approaches [18]. Jing et al. proposed an on-chip piezoresistive-sensor nonlinearity correction method with highly robust Class-AB driving capability, demonstrating that hardware-software co-design can reduce sensor nonlinearity to 4% of its original value [19]. These findings confirm that neural network methodologies possess robust nonlinear approximation capabilities and data-driven modeling prowess, making them well-suited for nonlinear angle inversion and error compensation in reflective fiber optic angle sensors.

Despite these advances, three major research gaps remain in the context of PV tracking mount angle monitoring:

(1) **Insufficient integration of mechanical linearization with AI-driven compensation.** Existing reflective fiber optic angle sensors predominantly rely on direct mirror-tilting or lever mechanisms [4,5], where the reflected light intensity decays nonlinearly over large angular swings. Few studies have introduced a "line-to-line" gear-rack conversion to linearize the angular-to-displacement relationship prior to optical interrogation, nor have they systematically combined this mechanical linearization with cascaded neural network compensation.

(2) **Lack of dedicated angle sensing solutions for distributed PV tracking arrays.** While FBG-based tilt sensors [8–10] offer high precision and temperature self-compensation, they require wavelength interrogation units that are costly when deployed per tracking unit. Plastic optical fiber goniometers [5] are low-cost but lack the measurement range (typically <140°) and accuracy needed for monopolar tracking mounts whose rotation can exceed 200°.

(3) **Inadequate residual error refinement under field conditions.** Single-stage neural networks [3,11,12] can capture global nonlinear trends but leave residual errors of 1°–3° in local angular ranges. Two-stage neural network calibration has been proven effective for proximity sensors—where a simple fully-connected layer computes an approximate distance and upper-layer weights are refined to achieve approximately 20× higher accuracy than conventional single-network methods [20]—but this cascaded coarse-to-fine philosophy has not been adapted to reflective fiber optic angle inversion with voltage and preliminary angle as joint inputs.

To bridge these gaps, this paper makes the following research contributions:

(1) **A novel "line-to-line" reflective fiber optic angle sensor architecture** is designed for oblique single-axis PV tracking mounts. A gear-rack mechanism converts the main shaft rotation angle into linear displacement of a mirror, mitigating the nonlinear reflectance decay inherent in direct mirror-tilting

(e.g., micro-displacement without gear-rack mechanisms) approaches [4,5] and providing a more stable baseline for AI compensation.

(2) **A two-stage neural network nonlinear modeling and error compensation method** is proposed. The first stage establishes a voltage-to-angle inversion model using a feedforward neural network; the second stage constructs a residual compensation network that takes both output voltage and preliminary predicted angle as inputs to perform secondary refinement of prediction residuals-extending the cascaded coarse-to-fine compensation philosophy of Kitamura et al. [20] to reflective fiber optic angle sensing.

(3) **Comprehensive experimental validation** demonstrates that the proposed method reduces the average nonlinear error from 31.96% (uncompensated) to 1.00% (basic neural network) and further to 0.31% (two-stage compensation), with a maximum absolute error of 1.4° on an independent measurement dataset-meeting the sub-degree accuracy requirement for PV tracking systems.

Based on the aforementioned analysis, this paper designs a reflective fiber-optic angle sensor and proposes a nonlinear modeling and error compensation method based on a two-stage neural network to address the monitoring requirements for spindle rotation angles in oblique single-axis photovoltaic tracking systems. First, a gear-rack mechanism converts the spindle rotation angle into linear displacement of the mirror, while reflective fiber optics capture variations in reflected light intensity and convert them into voltage signals. Distinct from conventional optical lever systems that rely on direct mirror tilting [4,5], this study introduces a gear-rack linkage to convert rotation into linear translation. This 'line-to-line' conversion mitigates errors caused by non-linear reflectance decay over large angular swings, providing a more stable baseline for AI compensation. Second, a neural network angle inversion model is established with sensor output voltage as input and standard angular values as output, replacing traditional linear fitting methods to directly characterize the nonlinear relationship between output voltage and rotation angle. Finally, an error compensation model is developed using preliminary angle predictions to perform secondary correction of prediction residuals, thereby further reducing measurement deviations caused by nonlinear light intensity effects, mechanical transmission errors, and environmental disturbances. Experimental data validate the proposed approach, demonstrating its effectiveness and practical value in monitoring rotation states of photovoltaic tracking systems.

2 Design of a Reflective Fiber Optic Angle Monitoring Sensor for Diagonal Single-Axis Photovoltaic Tracking Mounts

The oblique single-axis photovoltaic tracking mount adjusts the module inclination angle by rotating the drive shaft, enabling the photovoltaic modules to achieve optimal incidence angles at different times, as shown in Fig. 1.

To achieve real-time monitoring of the rotation angle of the support frame's main shaft, this paper designs a reflective fiber-optic angle sensing sensor, whose structure is shown in Fig. 2. The sensor consists primarily of a rotating shaft, a gear, a rack, a sliding rail, a sliding groove, a limiter, a reflector, a reflective fiber optic cable, a laser transmitter, and a laser receiver. The rotating shaft is coaxially connected to the main shaft of the photovoltaic tracking support frame and is used to measure the actual rotation angle of the support. The gear is mounted at the lower end of the rotating shaft and rotates synchronously with it. The rack is installed on the sliding rail and moves linearly along the sliding groove. A reflector is fixed at the end of the rack and serves to adjust the relative distance between the rack and the reflective fiber optic probe.

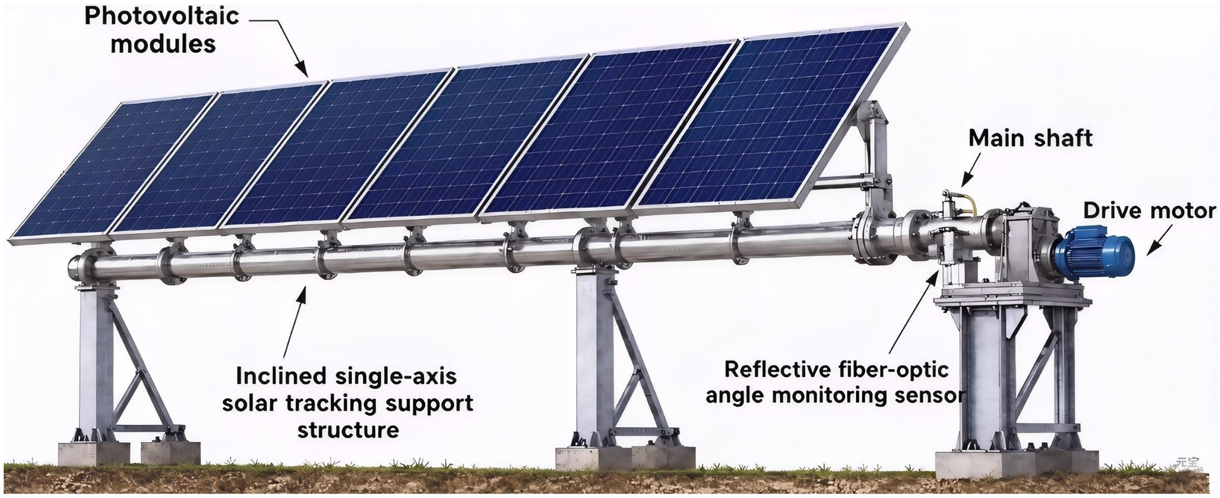

Figure 1: Schematic diagram of light angle sensor installation.

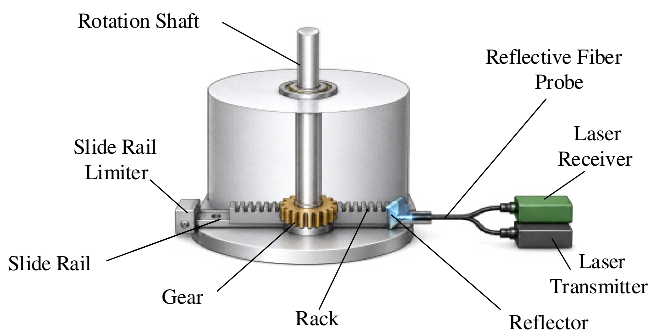

Figure 2: Schematic diagram of the structure of a reflective optical fiber angle sensor.

This sensor employs a structural conversion principle of "using straight lines instead of curves", transforming the rotational angle of the photovoltaic bracket's main shaft into linear displacement of the rack. When the main shaft rotates, the gear drives the rack to move along the guide rail, altering the position of the reflector relative to the optical fiber probe. The light signal emitted by the laser transmitter is transmitted via the transmitting fiber to the probe end face and strikes the reflector surface; the reflected light is then transmitted through the receiving fiber to the laser receiver, where it is converted into a corresponding voltage signal. This establishes a relationship between the main shaft rotation angle, rack displacement, reflected light intensity, and output voltage.

In a mechanical transmission system, let the radius of the gear's pitch circle be r, the rotation angle of the support shaft be θ, and the linear displacement of the rack be x. When the gear and rack are in a non-sliding engagement state, the following relationship holds between them:

$$x = r\theta \tag{1}$$

In this formula, θ is expressed in radians. Eq. (1) indicates that, for a given gear pitch radius, the rotation angle of the photovoltaic tracking mount can be determined from the linear displacement of the rack. To improve measurement stability under outdoor operating conditions, the rack is guided by a sliding rail and groove, while a mechanical limiter restricts its travel within the effective stroke. Consequently, the measurement performance of the proposed sensor is jointly determined by its mechanical transmission parameters and optical sensing characteristics. The main prototype parameters used in this study are summarized in Table 1.

Table 1: Main mechanical and optical parameters of the prototype.

Parameter	Value
Gear module	Actual value
Gear pitch radius	15 (mm)
Guide rail positioning tolerance	0.5 (mm)
Reflective fiber-optic probe model	Actual model
Laser wavelength	650 (nm)
Probe working distance	30 (mm)
Laser source stability	Actual specification

The parameters listed in Table 1 define the mechanical transmission characteristics and optical sensing conditions of the prototype and were used throughout the subsequent calibration and experimental evaluation.

3 Nonlinear Linear Compensation

3.1 Nonlinear Error Analysis

The sensor output voltage is primarily determined by the relative distance between the mirror and the reflective fiber optic probe. When the rotation axis undergoes angular displacement, the gear drives the rack to produce linear displacement, altering the distance between the mirror and the probe, which in turn affects the reflected light intensity at the receiver and the output voltage. Under ideal conditions-with zero clearance in the gear-rack transmission and a linear relationship between reflected light intensity and displacement-the sensor output voltage would exhibit a well-defined linear relationship with the rotation angle. However, in practical measurements, reflected light intensity exhibits significant nonlinearity as distance changes; additionally, factors such as machining errors, gear meshing clearance, mirror installation angle deviation, ambient light interference, and photoelectric conversion circuit drift all contribute to nonlinear deviations between the output voltage and the actual rotation angle.

To analyze the sensor output characteristics, an experimental data acquisition system as shown in Fig. 3 was established. In this system, a high-precision Hall angle sensor is used as a reference to collect angular data from the optical fiber angle sensor.

To evaluate the nonlinear characteristics of the proposed sensor, two different experimental datasets were acquired. The first dataset consisted of ten repeated forward–reverse measurements performed over the practical operating range of 0°–90°, which was used to analyze the nonlinear output characteristics, repeatability, and hysteresis of the sensor. The second dataset covered the full calibrated mechanical range of 0°–208.4° and was used for nonlinear model calibration and subsequent accuracy evaluation. Therefore, the ranges reported in Fig. 4 and the subsequent calibration results correspond to different experimental objectives rather than inconsistent measurement ranges.

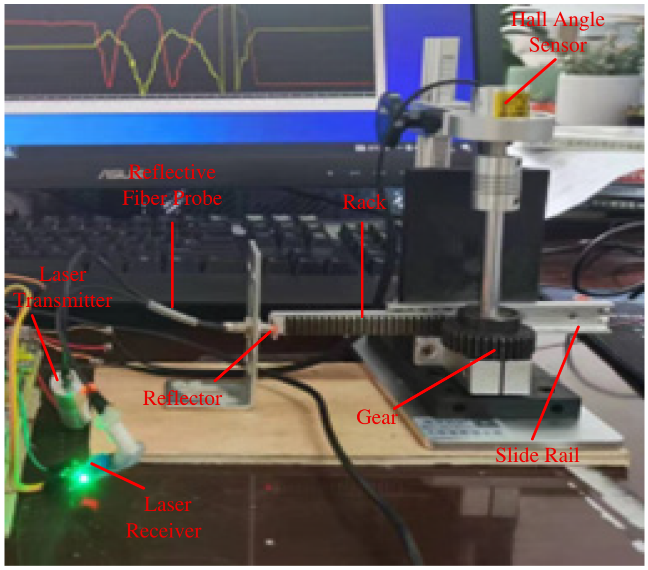

Figure 3: Data acquisition platform.

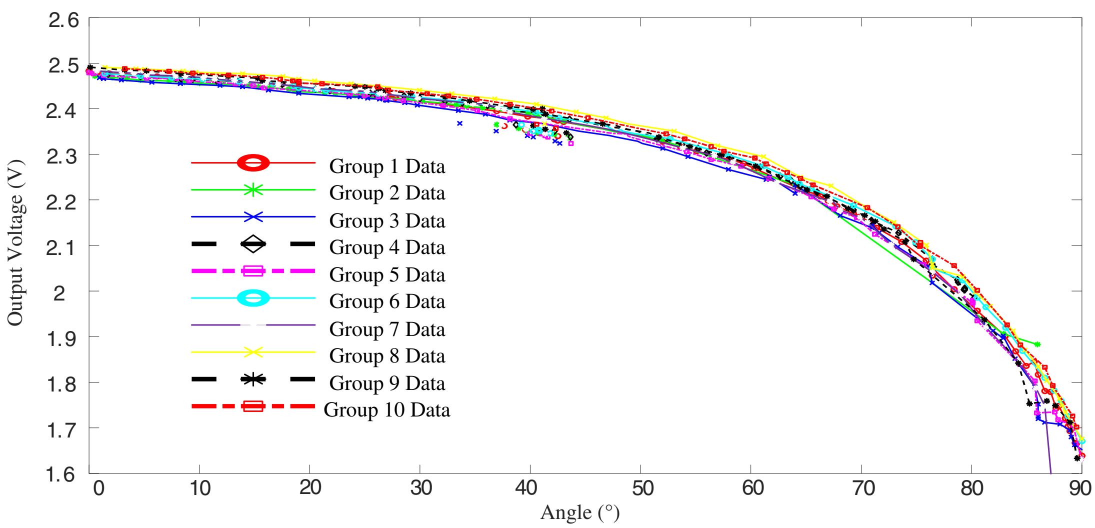

Figure 4: Voltage-angle characteristic curve of a reflective fiber optic angle sensor.

Under ideal conditions, the sensor output should maintain a proportional relationship with the input. However, in practice, this relationship often deviates from being perfectly linear due to interference from various external factors such as lighting environment, temperature and humidity, and mechanical structure. Fig. 4 illustrates the data curve obtained during the experiment.

Fig. 4 presents the voltage-angle curves obtained from ten repeated forward–reverse measurements over the practical operating range of 0°–90°. These measurements were used to evaluate the nonlinear output characteristics of the proposed sensor before neural-network modeling. It is evident that the sensor's output exhibits nonlinear characteristics with poor linearity.

The sensor nonlinear error can be used to quantify the deviation between actual output characteristics and ideal linear output, expressed as [21]:

$$\alpha_L = \frac{|\Delta\theta_m|}{Y\left(FS\right)} \times 100\% \tag{2}$$

In this formula α_L represents the nonlinear error, $\triangle\theta_m$ denotes the maximum fitting deviation, and $Y(FS)$ indicates the sensor's full-scale value. This parameter reflects the maximum degree of nonlinear deviation across the entire measurement range. For the reflective fiber optic angle sensor designed in this study, due to the complex nonlinear relationship between output voltage and angle, it is necessary to develop data-driven nonlinear angle inversion models and error compensation models.

3.2 Inverse Model from the Perspective of Neural Networks

Artificial neural networks possess strong capabilities for approximating nonlinear functions and can learn complex nonlinear mapping relationships from input and output samples without explicitly establishing physical analytical models [22]. The hidden layer comprises 15 neurons, optimized via grid search to balance computational cost and accuracy. The ReLU activation function was selected over Tanh to avoid vanishing gradient issues during backpropagation. To address the nonlinear relationship between the output voltage of a reflective optical fiber angle sensor and its rotation angle, this paper develops a neural network-based angle inversion model that uses the sensor's output voltage as input and standard angular values as output, directly establishing the following nonlinear mapping relationship:

$$\theta_\mathrm{i} = f_\mathrm{NN}\left(U_\mathrm{i}\right) \tag{3}$$

In this formula, θ_i represents the predicted angle output by the neural network model, and $f_\mathrm{NN}(\cdot)$ denotes the nonlinear mapping function learned by the neural network.

The angle inversion network developed in this paper adopts a three-layer feedforward neural network architecture with 15 neurons in the hidden layer. This specific count was determined via a grid search optimization process to balance model complexity and generalization capability, effectively preventing overfitting while capturing the sensor's nonlinear characteristics, as shown in Fig. 5, comprising an input layer, a hidden layer, and an output layer. The input layer contains one node corresponding to the output voltage U of the reflective optical fiber angle sensor; the output layer contains one node corresponding to the predicted angle θ; the hidden layer extracts nonlinear features between the output voltage and the angle; its neurons employ nonlinear activation functions, while the output layer uses linear activation functions to accommodate the continuous nature of angle values.

For the j-th neuron in the hidden layer, its output can be expressed as:

$$h_\mathrm{j} = g\left(w_\mathrm{j} U + b_\mathrm{j}\right) \tag{4}$$

In this formula, h_j denotes the output of the j-th neuron in the hidden layer; w_j represents the connection weight from the input layer to the hidden layer; b_j is the bias of the hidden layer; and $g(\cdot)$ is the activation function. The predicted value at the output layer can be expressed as:

$$\theta = \sum_{\mathrm{j}=1}^{m} u_\mathrm{j} h_\mathrm{j} + c \tag{5}$$

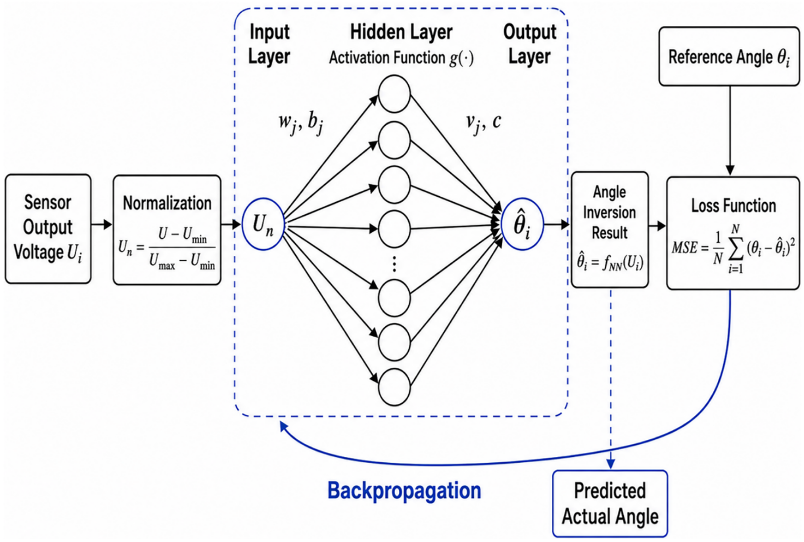

Figure 5: Inverse modeling from the perspective of neural networks.

In this formula, m represents the number of neurons in the hidden layer, u_j denotes the connection weights from the hidden layer to the output layer, and c is the bias of the output layer. To enhance network training stability, input voltages and reference angles are normalized prior to model training. Let the original voltage be U and the normalized voltage be U_n; then:

$$U_n = \frac{U - U_{min}}{U_{max} - U_{min}} \tag{6}$$

In the formula, U_{min} and U_{max} represent the minimum and maximum values of the sample voltage, respectively. The angle output is also normalized; after the network completes its prediction, inverse normalization is performed to obtain the actual predicted angle value.

The network training uses the mean square error between the predicted angle and the standard angle as the loss function, expressed as:

$$MES = \frac{1}{n}\sum_{i=1}^{n}\left(\theta_i - \hat{\theta}_i\right) \tag{7}$$

In this formula, θ_i represents the standard angle value, while $\hat{\theta}_i$ denotes the angle value predicted by the neural network. By continuously adjusting the network weights and biases using the backpropagation algorithm, the loss function is gradually minimized, thereby yielding an angle inversion model that accurately describes the nonlinear input-output relationship of the sensor.

The overall testing performance of the model is as follows: the Mean Absolute Error (MAE) [23] is 0.6682°, the Root Mean Square Error (RMSE) [23] is 0.9845°, the Max Absolute Error over the full measurement range (MAEmax) [23] is 3.1475°, and the coefficient of determination R^2 = 0.9997, indicating that the neural network accurately captures the overall trend of voltage-angle variations. Similar nonlinear optimization strategies have been proven effective in other angle sensing domains, such as vertical brushless electric power steering angle sensors [24]. As shown by the fitting curve on the right side of Fig. 6, the neural network's inversion curve closely matches the actual discrete experimental data. However, the prediction error curve on the left side reveals significant fluctuations across the entire measurement range, with peak single-point errors reaching up to 3.1475° in the low-angle measurement region. This demonstrates that the basic inversion model can only correct most nonlinear distortions of the sensor, while residual nonlinear errors persist, failing to meet high-precision angle measurement requirements.

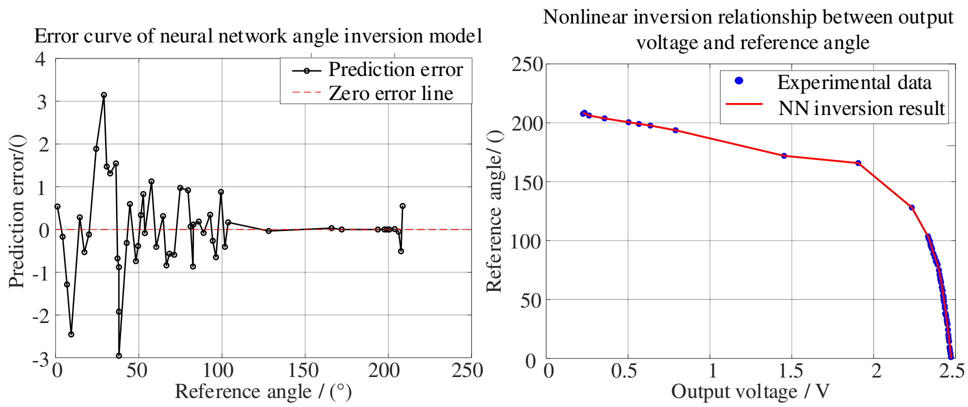

Figure 6: Comparison of fitting curves and prediction error curves for the neural network-based inversion model.

To quantify the nonlinearity of the fundamental inversion model, 15 typical calibration samples were uniformly selected across the entire measurement range using a measured calibration dataset. The measured reference angles were compared with those calculated by the neural network; the results are presented in Table 2.

Table 2: Comparison between the measured reference angle and the angle calculated by neural network inversion.

Order Number	Measured Voltage: U/V	Actual Reference Angle $\theta/(°)$	Basic Model Inversion Angle $\theta/(°)$	Abosolute Deviation $\Delta\theta = \hat{\theta} - \theta$
1	2.483	0.00	0.89	0.89
2	2.469	16.00	15.02	0.98
3	2.454	35.00	36.15	1.15
4	2.424	55.60	54.36	1.24
5	2.395	73.90	75.29	1.39
6	2.354	94.10	92.67	1.43
7	2.316	107.30	108.78	1.48
8	2.218	130.10	128.57	1.53
9	2.108	147.40	149.05	1.65
10	1.901	166.10	164.39	1.71
11	1.666	177.80	179.55	1.75
12	1.239	180.70	178.92	1.78
13	0.898	190.30	192.14	1.84
14	0.552	199.20	201.13	1.93
15	0.236	208.40	206.32	2.08

As shown in Table 2, the fundamental neural network angle inversion model effectively captures the nonlinear mapping relationship between sensor output voltage and measured reference angles. Among the

15 selected typical calibration samples, the absolute deviations between inverted angles and actual reference angles remained within a narrow range overall, with the minimum absolute deviation being 0.89° and the maximum observed in Sample 15 at 2.08°. According to Eq. (2), the nonlinear error of this model is approximately 1.00%, indicating its satisfactory performance in nonlinear angle inversion for reflective fiber optic sensors. However, Table 2 also reveals residual deviations in certain wide angular ranges, necessitating the development of a neural network error compensation model to perform secondary refinement on the initial inversion results and further enhance sensor measurement accuracy.

Both stages employed fully connected multilayer perceptrons (MLPs). The first-stage network consisted of one input neuron, one hidden layer with 12 neurons, and one output neuron (1-12-1). The second-stage residual network adopted a 2-10-1 architecture. The hidden layer used the hyperbolic tangent activation function, whereas the output layer employed a linear activation function. Both networks were trained using the Adam optimizer with an initial learning rate of 0.001. The maximum number of training epochs was set to 1000, and early stopping with a patience of 50 epochs was adopted to avoid overfitting. All input variables were normalized using min-max normalization before training. Seven repeated measurement sequences were used for training, one sequence for validation, and two sequences for independent testing.

3.3 Neural Network Error Compensation Model

While the neural network-based angle inversion model significantly enhances prediction accuracy, preliminary results may still exhibit residual errors due to limited experimental samples, mechanical hysteresis, and environmental disturbances. To further improve sensor measurement precision, this study develops a neural network error compensation model [25] built upon the original angle inversion framework, enabling secondary refinement of initial predictions.

First, from the perspective of neural networks, the initial $\hat{\theta}$ predicted angle is obtained by inverse modeling, and its residual with respect to the standard angle θ_i is calculated:

$$e = \theta - \hat{\theta} \tag{8}$$

In this formula, e represents the predicted residual at the i-th sample point. The error compensation model is then trained using the sensor output voltage U and the preliminary predicted angle θ as inputs, with the predicted residual e as the output, thereby establishing a residual compensation mapping relationship:

$$\hat{e} = f_{\text{MLP}}\left(U, \hat{\theta}\right) \tag{9}$$

In this formula $\hat{e}$, represents the residual compensation value predicted by the neural network error compensation model, and $f_{\text{MLP}}(\cdot)$ denotes the nonlinear mapping function learned by the error compensation network.

After obtaining the residual compensation value, adjust the preliminary predicted angle to obtain the final compensated angle:

$$\theta' = \hat{\theta} + \hat{e} \tag{10}$$

In this formula $\hat{\theta}$, represents the final angular output value after error compensation by the neural network.

The fundamental workflow of this two-stage neural network compensation method is as follows: first, an angle inversion network is employed to perform a preliminary nonlinear mapping from output voltage to angle; then, an error compensation network learns the variation patterns of the initial prediction errors and applies a secondary correction to the predictions. This approach separates the sensor's nonlinear modeling process from the residual correction process, enabling the model to not only capture overall nonlinear trends but also refine prediction deviations within specific angular ranges, as illustrated in Fig. 7.

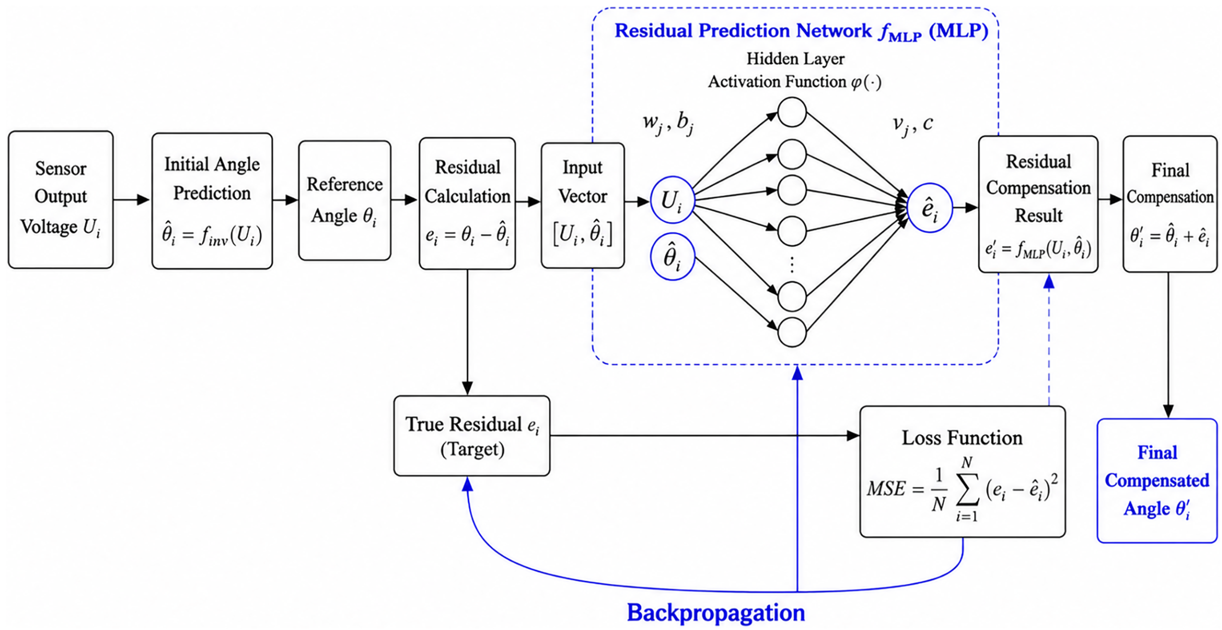

Figure 7: Neural network error compensation model.

To evaluate the correction performance of the neural network error compensation model on foundation angle inversion results, measured voltage values, measured reference angles, and inversion angles from the basic model in Table 2 were used as compensation inputs. The measured voltage U_i and the basic model's inversion angle θ_i served as the input to the error compensation network, while the fundamental inversion residual e_i was designated as the network output target. After training, the network produced residual prediction values, and the final compensated angle was calculated using Eq. (10). Table 3 presents the corrected angles and their corresponding deviations after neural network-based error compensation.

As shown in Table 3, after neural network error compensation, the deviation between the compensated angle and the measured reference angle further decreases. The maximum absolute deviation of the basic neural network angle inversion model was 2.08° before compensation, which dropped to 0.64° afterward, demonstrating that the error compensation network effectively learns the variation patterns of residuals in the basic inversion model and performs a secondary correction on the preliminary prediction results. Compared with the single-neural-network angle inversion model, the two-stage neural network approach not only establishes a nonlinear mapping relationship between output voltage and angle but also further corrects residual errors within specific local ranges, thereby enhancing the overall measurement accuracy of the sensor.

Table 3: Angle error analysis after neural network error compensation.

Order Number	Measured Voltage (U/V)	Actual Reference Angle ($\theta/(^\circ)$)	Basic Model Inversion Angle ($\theta/(^\circ)$)	Compensated Angle ($\theta'/^\circ$)	Absolute Deviation ($\lvert\Delta\ \theta\rvert/(^\circ)$)
1	2.483	0	0.89	0.18	0.18
2	2.469	16	15.02	16.21	0.21
3	2.454	35	36.15	34.76	0.24
4	2.424	55.6	54.36	55.88	0.28
5	2.395	73.9	75.29	73.59	0.31
6	2.354	94.1	92.67	94.43	0.33
7	2.316	107.3	108.78	106.94	0.36
8	2.218	130.1	128.57	130.49	0.39
9	2.108	147.4	149.05	146.97	0.43
10	1.901	166.1	164.39	166.56	0.46
11	1.666	177.8	179.55	177.31	0.49
12	1.239	180.7	178.92	181.23	0.53
13	0.898	190.3	192.14	189.74	0.56
14	0.552	199.2	201.13	198.59	0.61
15	0.236	208.4	206.32	207.76	0.64

According to Eq. (2), the nonlinear error after neural network error compensation is 0.31%, a reduction of 0.69 percentage points. This demonstrates that the proposed neural network error compensation model effectively improves the nonlinear output characteristics of reflective fiber optic angle sensors across the entire measurement range, enhancing both the accuracy and stability of angle measurements.

To provide a more intuitive analysis of the correction effectiveness of the neural network error compensation model, comparison curves illustrating angular errors before and after compensation were plotted based on the angle data in Tables 2 and 3, as shown in Fig. 8. The figure demonstrates that the basic neural network inversion model still exhibits certain prediction deviations at each reference point, with relatively large errors in certain wide-angle ranges; after correction by the error compensation network, errors at all reference points significantly decreased, and the error curves generally approached the zero-error baseline. The maximum absolute error was 2.08° before compensation, dropping to 0.64° afterward, indicating that the error compensation network effectively learns the variation patterns of residuals from the basic inversion model and performs a secondary refinement of angular predictions.

4 Experimental Analysis

4.1 Analysis of Nonlinear Compensation Experimental Results

To verify the effectiveness of the proposed two-stage neural network compensation method, this study focuses on monitoring the main shaft rotation angle of a tilted single-axis photovoltaic tracking mount. Both a reflective fiber optic angle sensor and a high-precision Hall angle sensor were installed at the end of the tracking mount's main shaft. The Hall angle sensor measurements served as the reference angle, while the output voltage from the reflective fiber optic sensor was used as input to the neural network model. Multiple sets of experimental data were fed into four different approaches-including the look-up table method [26], the polynomial fitting method, the BP neural network method [26], and the proposed two-stage neural network method-for nonlinear compensation comparisons, yielding the corresponding nonlinear error results as shown in Table 4.

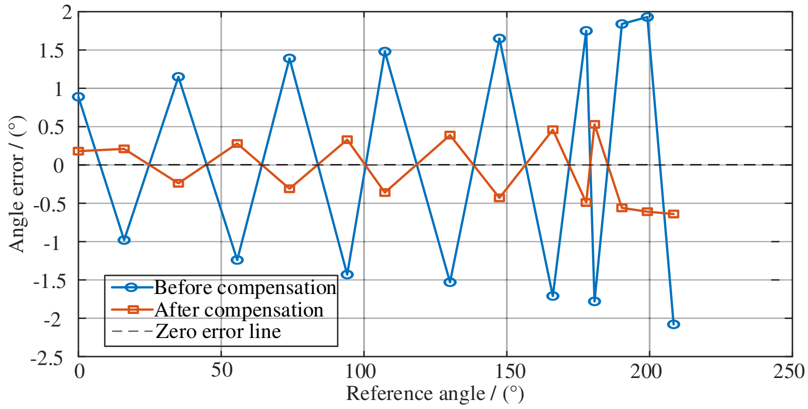

Figure 8: Comparison curve of angular error before and after compensation.

Table 4: Comparison of nonlinear errors under different compensation methods.

Experimental Group	Not Compensated	Look-Up Table	Polynomial Fitting Method	BP Neural Network Method	Basic Neural Network Inversion Method	Two-Stage Neural Network Method
1	32.01%	9.84%	11.26%	6.12%	1.00%	0.31%
2	31.68%	9.56%	10.93%	6.04%	1.03%	0.33%
3	32.45%	10.18%	11.51%	6.36%	0.98%	0.30%
4	31.92%	9.73%	11.08%	6.21%	1.02%	0.32%
5	31.75%	9.61%	10.87%	6.08%	0.97%	0.29%
Average value	31.96%	9.78%	11.13%	6.16%	1.00%	0.31%

The look-up table method used linear interpolation between adjacent calibration nodes. The polynomial fitting method employed a least-squares regression to model the nonlinearity in software. The BP neural network was implemented according to Literature [27] using a conventional single-stage neural network. The proposed basic neural network represents the first-stage nonlinear inversion model developed in this work, whereas the proposed two-stage model further introduces a residual compensation network for secondary correction.

Fig. 9 presents a comparison of average nonlinear errors under different compensation methods. The figure shows that the average nonlinear error of the sensor without compensation is 31.96%, indicating a significant nonlinear relationship between the output voltage of the reflective fiber angle sensing sensor and the main shaft rotation angle. While the table lookup method, polynomial fitting approach, and BP neural network method all reduced nonlinear errors to some extent—averaging 9.78%, 11.13%, and 6.16%, respectively—the fundamental neural network inversion model demonstrated superior performance by accurately capturing the nonlinear relationship between output voltage and rotation angle, reducing the average error to 1.00%. Building on this, the two-stage neural network method further incorporated an error compensation network to perform secondary correction on initial inversion residuals, further lowering the average nonlinear error to 0.31%. These results demonstrate that the proposed two-stage neural network compensation method exhibits enhanced capability in correcting nonlinear errors.

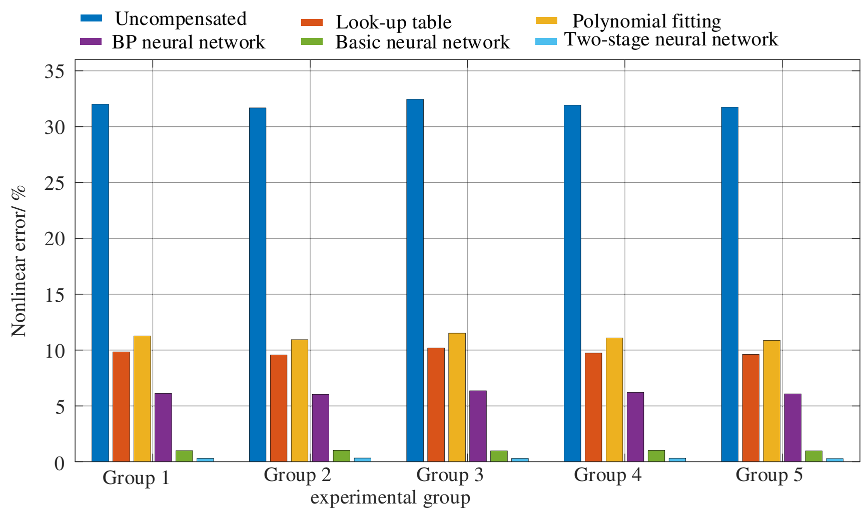

Figure 9: Comparison of nonlinear errors for different compensation methods.

4.2 Measurement Error Analysis

To verify the measurement accuracy of the reflective fiber-optic angle-monitoring sensor in photovoltaic tracking mount systems, it was installed alongside a high-precision Hall angle sensor on the main axis of a tilted single-axis tracking mount for simultaneous measurements. Using the Hall sensor's output angle as the reference value, the measurement error between the two was calculated. It is worth noting that the training dataset for the neural network incorporated variations in ambient light intensity and temperature to ensure the model remains robust against common outdoor environmental interferences. Selected measurement results are presented in Table 5.

Table 5: Comparison of measurement results between Fiber-optic angle detection sensor and Hall angle sensor.

Number of Experiments	Hall Angle Sensor/(°)	Fiber Optic Turn Detection Sensor/(°)	D-Value/(°)
1	0	0.2	0.2
2	15	15.4	0.4
3	30	29.5	−0.5
4	45	45.6	0.6
5	60	59.4	−0.6
6	75	75.7	0.7
7	90	89.3	−0.7
8	120	121	1
9	150	148.9	−1.1
10	180	181.2	1.2
11	200	198.7	−1.3
12	208.4	207	−1.4

Fig. 10 compares the measurement results of a Hall angle sensor and a reflective fiber-optic angle-monitoring sensor. As shown, the compensated measurements from the fiber-optic sensor exhibit good consistency with the reference values obtained from the Hall angle sensor, demonstrating that the proposed two-stage neural network compensation method effectively enhances the angular measurement accuracy of reflective fiber-optic sensors.

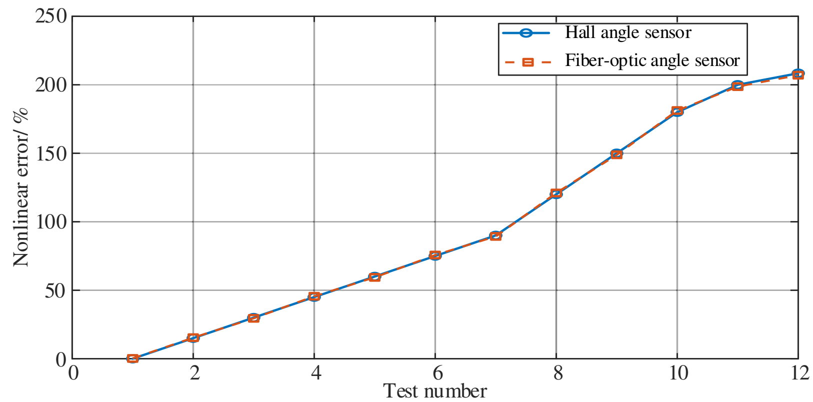

Figure 10: Comparison of measurement angles between fiber-optic sensor and hall sensor.

Experimental data analysis reveals that the maximum absolute error of the compensated sensor is 1.4°, with a Mean Absolute Error (MAE) of 0.81° and a Root Mean Square Error (RMSE) of 0.89°. These results demonstrate that the designed reflective fiber-optic angle-monitoring sensor meets the fundamental requirements for tracking the rotation state of inclined single-axis photovoltaic tracking mounts.

The error indices reported in this section were obtained from an independent measurement dataset that was not used for model calibration or parameter tuning, whereas the results in Table 2 represent the fitting accuracy on representative calibration points.

During repeated forward and reverse measurements, the major source of hysteresis originated from gear backlash and rack friction. Larger deviations mainly appeared near the reversal positions, whereas the remaining angle range showed relatively stable performance. Although the proposed neural-network compensation effectively reduced systematic nonlinear errors, random mechanical hysteresis caused by backlash and friction could not be completely eliminated.

4.3 Engineering Applications and Economic Analysis

Diagonal single-axis photovoltaic tracking mounts are typically deployed over extensive areas and require a large number of installations. Using high-precision optical encoders or complex servo angle measurement systems for each tracking unit would significantly increase equipment costs and maintenance requirements. In contrast, the reflective fiber-optic angle-monitoring sensor designed in this paper consists primarily of a gear-rack mechanism, reflective fiber optics, a laser transmitter, and a laser receiver, featuring a relatively simple structure without complex electrical components at the sensing end. It offers strong immunity to electromagnetic interference, facilitates long-distance signal transmission, and is well-suited for outdoor distributed installations.

From an engineering application perspective, traditional potentiometric angle sensors are cost-effective but prone to mechanical wear and contact noise during long-term operation; optical encoders offer high measurement accuracy but are expensive and require strict coaxial alignment and protective conditions; Hall effect angle sensors provide excellent non-contact measurement capabilities, yet still face challenges with magnetic interference and packaging protection in complex electromagnetic environments and prolonged outdoor operation, as shown in Table 6. The reflective fiber optic angle monitoring sensor proposed in this paper achieves high measurement accuracy while reducing dependence on field-based electrical measurement units, making it suitable for long-term online monitoring of main shaft angles in photovoltaic tracking systems [28]. Given the non-contact nature of the optical fiber probe and the sealed design of the gear-rack mechanism, the estimated service life of the proposed sensor is over 10 years, significantly reducing the replacement frequency required for traditional contact-based sensors. The enclosure is rated IP67, ensuring stable operation in dusty and rainy environments typical of desert photovoltaic bases. Fibre-optic sensing combined with deep learning has been widely recognized as a powerful paradigm for structural health monitoring in harsh outdoor environments [29,30], further validating the architectural choice of this study.

Table 6: Comparison of engineering applications for different sensor implementation approaches.

Sensing Scheme	Certainty of Measurement	Anti-Electromagnetic Interference Capability	Outdoor Adaptability	Installation Complexity	Cost Level	Maintenance Requirements
Potentiometer-Type Angle Sensor	Moderate	Moderate	Moderate	Low	Low	Relatively high
Hall Angle Sensor	Relatively high	Medium	Relatively high	Medium	Medium	Medium
Photoelectric Encoder	High	Relatively high	Relatively high	Relatively high	High	Medium
Reflective Optical Fiber Angle Sensor	Relatively high	High	Relatively high	Medium	Medium	Relatively low

Fig. 11 presents a comparison of the engineering applicability of various angle sensing solutions for monitoring rotation angles of photovoltaic tracking mounts. For comprehensive evaluation, this study quantifies each solution across five criteria: cost-effectiveness, installation convenience, interference resistance, outdoor adaptability, and maintenance ease, with scores ranging from 0 to 10 (higher scores indicate better performance). As shown in Fig. 11, potentiometric angle sensors demonstrate advantages in cost and installation simplicity but exhibit lower interference resistance and maintenance requirements, making them less suitable for long-term stable outdoor monitoring. Hall effect angle sensors offer balanced performance but remain susceptible to interference in complex electromagnetic environments. Optical encoders provide high measurement accuracy but come with higher costs, stringent coaxial installation requirements, and greater field maintenance complexity [31]. In contrast, reflective fiber optic angle sensors excel in interference resistance and maintenance convenience while offering superior outdoor adaptability and moderate-to-low engineering costs. Overall, this solution is particularly suitable for large-scale distributed rotation monitoring of inclined single-axis photovoltaic tracking mounts, ensuring measurement accuracy while reducing on-site installation and maintenance burdens, demonstrating excellent practicality and cost-effectiveness throughout the entire lifecycle.

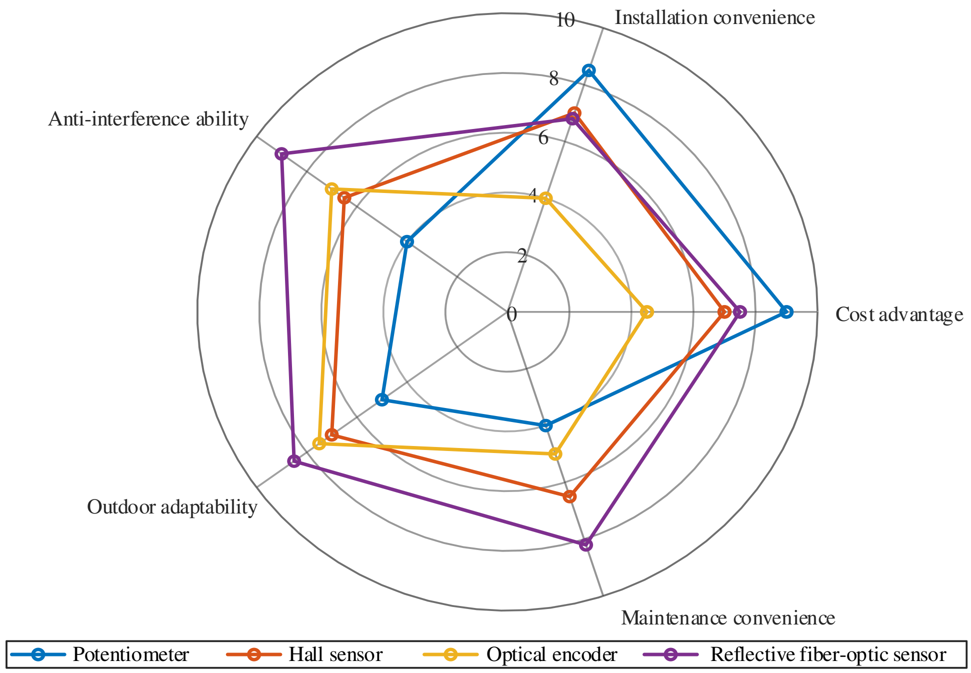

Figure 11: Comparison of engineering applicability of different angle sensing schemes.

It should be noted that all experiments reported in this study were conducted under controlled laboratory conditions. To reduce the influence of ambient illumination, the reflective fiber probe and reflector were enclosed in an opaque shielding structure during testing. No optical modulation/demodulation or ratiometric normalization was implemented in the current prototype. Therefore, the effects of long-term sunlight exposure, temperature variation, humidity, vibration, mirror contamination, and mechanical wear have not yet been quantitatively evaluated. These factors will be investigated through long-term outdoor experiments in future work.

Before field deployment, each sensor should undergo an initial multi-point calibration after installation to establish the voltage-angle relationship under its actual mechanical assembly conditions. Periodic recalibration is recommended to compensate for gradual performance degradation caused by mirror contamination and mechanical wear. Long-term outdoor validation has not yet been conducted and will be included in future work.

5 Conclusion

This paper addresses the monitoring requirements for spindle rotation angle states in oblique single-axis photovoltaic tracking mounts by designing a reflective fiber-optic angle sensing sensor and proposing a nonlinear angle inversion and error compensation method based on a two-stage neural network. The sensor converts the mount's spindle rotation angle into linear displacement of a reflective mirror via a gear-rack mechanism, generating voltage signals through variations in reflected light intensity. It features a simple structure, strong anti-interference capability, and suitability for outdoor distributed monitoring applications. To address the nonlinear relationship between output voltage and rotation angle, a neural network-based angle inversion model was first established to obtain preliminary prediction results, followed by secondary residual correction through an error compensation network. The proposed method achieved an MAE of 0.401° on representative calibration points and 0.81° on an independent measurement dataset, demonstrating both high fitting accuracy and satisfactory generalization capability. Engineering feasibility analysis confirms this sensing solution offers significant advantages in interference resistance, maintenance convenience, and outdoor adaptability, providing an effective technical solution for monitoring rotation states and ensuring safe operation of photovoltaic tracking systems. Although designed for photovoltaic trackers, the underlying principle of combining mechanical linearization with neural network compensation is readily transferable to other rotating machinery monitoring scenarios, including wind turbine pitch control and robotic joint positioning.

Acknowledgement: Not applicable.

Funding Statement: This research was funded by the Foundation of University-Enterprise Joint Application Technology Innovation Base of Smart Safety Monitoring of Urban Utility Tunnel at Chengdu Vocational & Technical College of Industry, grant number 2026GL-Z01. This research was also supported by Hebei Natural Science Foundation, grant number E2026502058.

Author Contributions: The authors confirm contribution to the paper as follows: conceptualization, Qingmin Hou and Tongtong Dai; methodology, Qingmin Hou; software, Guanghua Xiao; validation, Guanghua Xiao; formal analysis, Guanghua Xiao; investigation, Qingmin Hou; resources, Tongtong Dai; data curation, Guanghua Xiao; writing—original draft preparation, Qingmin Hou; writing—review and editing, Tongtong Dai; visualization, Tongtong Dai; supervision, Guanghua Xiao; project administration, Qingmin Hou; funding acquisition, Qingmin Hou. All authors reviewed and approved the final version of the manuscript.

Availability of Data and Materials: The data that support the findings of this study are available from the corresponding author upon reasonable request.

Ethics Approval: Not applicable.

Conflicts of Interest: The authors declare no conflicts of interest.

References

1. Sadeghi R, Parenti M, Memme S, Fossa M, Morchio S. A review and comparative analysis of solar tracking systems. Energies. 2025;18(10):2553. doi:10.3390/en18102553.
2. Sun Q, Gutiérrez JLR, Yu X. Deep neural network-based 4-quadrant analog sun sensor calibration. Space Sci Technol. 2023;3:24. doi:10.34133/space.0024.
3. Liu R, Li M, Zhang J, Han Z. Design and hysteresis compensation of novel resistive angle sensor based on rotary potentiometer. Sensors. 2025;25(13):4077. doi:10.3390/s25134077.
4. Zhang J, Gu Q, Wan P, Liu Y, Yang D, Li X. Optical fiber sensor used for measuring the rotation angle of the disconnecting switch. Sci Rep. 2025;15(1):5477. doi:10.1038/s41598-025-89310-8.
5. Lee HW, Kim DH, Shin S. Low-cost angle sensor for robotics applications using plastic optical fiber based on optical loss mechanism. Biomimetics. 2023;8(8):567. doi:10.3390/biomimetics8080567.
6. Jia B, He L, Yan G, Feng Y. A differential reflective intensity optical fiber angular displacement sensor. Sensors. 2016;16(9):1508. doi:10.3390/s16091508.
7. Luo Z, Liu R, Wu L, Ran J, Wang Y, Qin S, et al. Fiber angular displacement sensor utilizing orbital angular momentum beam interference. Opt Lett. 2025;50(8):2759–62. doi:10.1364/OL.558045.
8. Pan J, Wang L, Hou W, Lv H. Design and investigation of a high-sensitivity tilt sensor based on FBG. Photonic Sens. 2022;13(2):230228. doi:10.1007/s13320-022-0671-8.
9. Zhang R, Dou H, Zhang P, Liu J, Wu X. Dual-axis fiber Bragg grating tilt sensor based on universal joint structure. Opt Fiber Technol. 2024;87(7):103898. doi:10.1016/j.yofte.2024.103898.
10. Theophilus N, Guo YX, Zhou WH, Yu HS, Ren RH, Shen S. Design optimization of a sensitivity-enhanced tilt sensor based on femtosecond fiber Bragg grating. Chin Opt. 2025;18(4):908–20. doi:10.37188/co.en-2024-0034.

11. Li K, Zhang Z, Lin J, Sato R, Matsukuma H, Gao W. Angle measurement based on second harmonic generation using artificial neural network. Nanomanuf Metrol. 2023;6(1):28. doi:10.1007/s41871-023-00206-5.
12. Lin J, Zhang Z, Sato R, Li K, Mizutani Y, Matsukuma H, et al. GUM-based measurement uncertainty analysis of a nonlinear optical angle sensor using artificial neural network. Nanomanuf Metrol. 2025;8(1):21. doi:10.1007/s41871-025-00273-w.
13. Wei M, Liu Z. Research of neural network-based model for nonlinear temperature drift compensation of MEMS accelerometers. Rev Sci Instrum. 2024;95(11):115107. doi:10.1063/5.0223517.
14. Chen M, Geng S, Zheng F, He Y, Han J, Dai H, et al. Nonlinear error compensation for microfiber knot current sensors based on artificial neural network. Opt Fiber Technol. 2023;80(11):103459. doi:10.1016/j.yofte.2023.103459.
15. Cao L, Abedin S, Cui G, Wang X. Artificial intelligence and machine learning in optical fiber sensors: a review. Sensors. 2025;25(24):7442. doi:10.3390/s25247442.
16. Zhou Y, Zhang YN, Yu Q, Ren L, Liu Q, Zhao Y. Application of machine learning in optical fiber sensors. Measurement. 2024;228(1):114391. doi:10.1016/j.measurement.2024.114391.
17. Tritschler P, Ohms T, Yang B, Zimmermann A. Meta-learning for few-shot sensor self-calibration to increase stress robustness. Eng Appl Artif Intell. 2024;138(4):109171. doi:10.1016/j.engappai.2024.109171.
18. Fan Q, Zhang X, Wen Z, Xu L, Zhang Q. Nonlinear compensation of the linear variable differential transducer using an advanced snake optimization integrated with tangential functional link artificial neural network. Sensors. 2025;25(4):1074. doi:10.3390/s25041074.
19. Jing K, Han Y, Yuan S, Zhao R, Cao J. A piezoresistive-sensor nonlinearity correction on-chip method with highly robust class-AB driving capability. Sensors. 2024;24(19):6395. doi:10.3390/s24196395.
20. Kitamura R, Koyama K, Wan W, Harada K. High-speed high-precision calibration of proximity sensor using two stages NN model. Proc JSME Annu Conf Robot Mechatron. 2021;2021:2A1–J07. doi:10.1299/jsmermd.2021.2a1-j07.
21. Zhang Y, Liu F, Zhou Z, Liang X, Sun R, Deng J, et al. Near-zero nonlinear error pressure sensor based on piezoresistor sensitivity matching for wind tunnel pressure test. Microsyst Nanoeng. 2025;11(1):122. doi:10.1038/s41378-025-00959-7.
22. Reyes-Vera E, Valencia-Arias A, García-Pineda V, Aurora-Vigo EF, Alvarez Vásquez H, Sánchez G. Machine learning applications in optical fiber sensing: a research agenda. Sensors. 2024;24(7):2200. doi:10.3390/s24072200.
23. Liu Y, Ping M, Han J, Cheng X, Qin H, Wang W. Neural network methods in the development of MEMS sensors. Micromachines. 2024;15(11):1368. doi:10.3390/mi15111368.
24. Chen J, Guo Y. Design and non-linearity optimization of a vertical brushless electric power steering angle sensor. Sensors. 2024;24(8):2469. doi:10.3390/s24082469.
25. Lv B, Li S, Liu J. Harmonic suppression method for optical encoder based on photosensitive unit parameter optimization. Optics. 2025;6(4):62. doi:10.3390/opt6040062.
26. Rotar R, Petcuţ FM, Susany R, Opriţoiu F, Vlăduţiu M. Dependability assessment of a dual-axis solar tracking prototype using a maintenance-oriented metric system. Appl Syst Innov. 2024;7(4):67. doi:10.3390/asi7040067.
27. Wang L, Zhang J, Wan P, Liu Y, Yang D, Li X, et al. Research on measurement technology of optical fiber angle sensor based on MEA-BP. Sci Rep. 2026;16(1):16915. doi:10.1038/s41598-026-48008-1.
28. Jayawickrema UMN, Herath HMCM, Hettiarachchi NK, Sooriyaarachchi HP, Epaarachchi JA. Fibre-optic sensor and deep learning-based structural health monitoring systems for civil structures: a review. Measurement. 2022;199(3):111543. doi:10.1016/j.measurement.2022.111543.
29. Mahmood Y, Yasir N, Quenette K, Badin G, Huang Y, Xu L. Fiber-optic sensor-based structural health monitoring with machine learning: a task-oriented and cross-domain review. Sensors. 2026;26(9):2641. doi:10.3390/s26092641.
30. Golovastikov NV, Kazanskiy NL, Khonina SN. Optical fiber-based structural health monitoring: advancements, applications, and integration with artificial intelligence for civil and urban infrastructure. Photonics. 2025;12(6):615. doi:10.3390/photonics12060615.
31. Zhao Y, Zhang Y, Zhang H, Xue L, Ren M, Miao Y. Rotation angle measurement method based on self-mixing interference of a fiber laser. Appl Opt. 2022;61(11):3174–81. doi:10.1364/AO.451675.